Title

Thalamic atrophy in antero-medial and dorsal nuclei correlates with six-month outcome after severe brain injury.

Authors

Lutkenhoff, Evan S
McArthur, David L
Hua, Xue
et al.

Publication Date

2013

DOI

10.1016/j.nicl.2013.09.010

Peer reviewed

NeuroImage: Clinical 3 (2013) 396–404

Contents lists available at ScienceDirect

NeuroImage: Clinical

journal homepage: www.elsevier.com/locate/ynicl

Thalamic atrophy in antero-medial and dorsal nuclei correlates with six-month outcome after severe brain injury ☆

Evan S. Lutkenhoff [a], David L. McArthur [b], Xue Hua [c], Paul M. Thompson [c,d], Paul M. Vespa [b,e], Martin M. Monti [a,b,*]

[a] Department of Psychology, University of California Los Angeles, Los Angeles, CA 90095, USA
[b] Brain Injury Research Center (BIRC), Department of Neurosurgery, David Geffen School of Medicine at UCLA, Los Angeles, CA 90095, USA
[c] Laboratory of Neuro Imaging (LONI), Department of Neurology, David Geffen School of Medicine at UCLA, Los Angeles, CA 90095, USA
[d] Department of Psychiatry, University of California Los Angeles, Los Angeles, CA 90095, USA
[e] Department of Neurology, David Geffen School of Medicine at University of California Los Angeles, Los Angeles, CA 90095, USA

ARTICLE INFO

Article history:
Received 28 June 2013
Received in revised form 26 September 2013
Accepted 27 September 2013
Available online 5 October 2013

Keywords:
Traumatic brain injury
Thalamus
Tensor brain morphometry
Magnetic resonance imaging

ABSTRACT

The primary and secondary damage to neural tissue inflicted by traumatic brain injury is a leading cause of death and disability. The secondary processes, in particular, are of great clinical interest because of their potential susceptibility to intervention. We address the dynamics of tissue degeneration in cortico-subcortical circuits after severe brain injury by assessing volume change in individual thalamic nuclei over the first six-months post-injury in a sample of 25 moderate to severe traumatic brain injury patients. Using tensor-based morphometry, we observed significant localized thalamic atrophy over the six-month period in antero-dorsal limbic nuclei as well as in medio-dorsal association nuclei. Importantly, the degree of atrophy in these nuclei was predictive, even after controlling for full-brain volume change, of behavioral outcome at six-months post-injury. Furthermore, employing a data-driven decision tree model, we found that physiological measures, namely the extent of atrophy in the anterior thalamic nucleus, were the most predictive variables of whether patients had regained consciousness by six-months, followed by behavioral measures. Overall, these findings suggest that the secondary non-mechanical degenerative processes triggered by severe brain injury are still ongoing after the first week post-trauma and target specifically antero-medial and dorsal thalamic nuclei. This result therefore offers a potential window of intervention, and a specific target region, in agreement with the view that specific cortico-thalamo-cortical circuits are crucial to the maintenance of large-scale network neural activity and thereby the restoration of cognitive function after severe brain injury.

1. Introduction

Traumatic brain injury (TBI) is a leading cause of death and severe disability in the United States (Coronado et al., 2011; MacKenzie, 2000), and has long been projected to be a leading cause of death and disability in the world (Murray and Lopez, 1997). The principal mechanisms of TBI typically include focal brain damage due to contact injury types resulting in contusion, laceration, intracranial hemorrhage, and diffuse brain damage due to acceleration/deceleration injury types resulting in diffuse axonal injury (DAI) or brain swelling (Werner and Engelhard, 2007). However, the damage inflicted by TBI, as well as the potential outcome, crucially depends not only on the local effects of the primary insult, but also on the secondary, delayed, non-mechanical processes consequent to axonal damage and Wallerian degeneration (Hall et al., 2005). These secondary processes, which in humans can take from several hours to days (Christman et al., 1994), involve necrotic and apoptotic death cascades in brain regions distal to the primary site of the trauma, assumed to result from membrane failure and disruption of ionic homeostasis inducing rapid degradation of the neuronal cytoskeleton and its cytoplasmic constituents (Povlishock and Katz, 2005). This aspect of neuronal damage is particularly relevant in the clinical setting because, unlike the site of primary damage, which is typically only susceptible to preventive measures, secondary processes might be susceptible to therapeutic intervention (Werner and Engelhard, 2007). Understanding the mechanisms of secondary insult, as well as the regions of the brain most affected by it, might therefore offer novel strategies for therapeutic interventions in TBI survivors.

* Corresponding author at: University of California, Los Angeles, Department of Psychology, Los Angeles, Ca 90095, USA. Tel.: +1 310 825 8546; fax: +1 310 206 5895.
E-mail address: monti@psych.ucla.edu (M.M. Monti).

2213-1582/$ – see front matter © 2013 The Authors. Published by Elsevier Inc. All rights reserved.
http://dx.doi.org/10.1016/j.nicl.2013.09.010

One region of the brain particularly vulnerable to secondary mechanisms is the bilateral thalamus, an area that due to its central location is relatively more protected from direct impact in TBI (Fearing et al., 2008). Indeed, the thalamus has been shown in animal models to be a site of retrograde neuronal apoptosis after cortical damage (Martin et al., 2001; Natale et al., 2002) within the first few days post-trauma (Hall et al., 2005). The important role of the thalamus in TBI has also been shown by reports demonstrating associations between subcortical lesion volume and 1 to 4 years post-injury performance across several neuropsychological tests (Babikian et al., 2005). Furthermore, at the high end of severity, thalamic circuits are considered to play a central role in permanent vegetative states (Monti, 2012). Post-mortem examinations have shown that 80 to 100% of patients in permanent vegetative state exhibit widespread thalamic damage (Adams et al., 2000). Indeed, damage to the thalamo-cortical axis has been reported to be sufficient to induce a vegetative state (VS) even in the presence of intact cortico-cortical connectivity (Boly et al., 2009). Conversely, direct or indirect stimulation of the thalamus has been associated with functional improvements in both moderate (Kang et al., 2012) and severe (Schiff et al., 2007; Yamamoto et al., 2013) TBI survivors.

In what follows, we employ tensor-based morphometry (TBM; Thompson et al., 2000) to assess the dynamics of structural change within individual thalamic nuclei occurring between the acute and chronic phases of moderate to severe TBI. Tensor-based morphometry, a technique related to deformation-based morphometry (Ashburner et al., 1998), employs deformations obtained from nonlinear registration of two brain images (e.g., an individual anatomical image to a follow-up image, or to an anatomical template) to infer 3D patterns of statistical differences in brain volume or shape between two images (Ashburner and Friston, 2000; Ashburner et al., 1998; Chung et al., 2001, 2003; Wang et al., 2003). In the past 15 years, this technique has been successfully applied to measure structural neuroanatomical changes over time, including mapping of growth patterns in the developing brain (Chung et al., 2001; Thompson et al., 2000), degenerative rates in Alzheimer's disease and other forms of dementia (Fox and Freeborough, 1997; Fox et al., 1996, 1999, 2000, 2001; Freeborough and Fox, 1997; Freeborough et al., 1996; O'Brien et al., 2001; Studholme et al., 2001), as well as tumor growth (Lemieux et al., 1998) and multiple sclerosis lesions (Ge et al., 2000; Rey et al., 2002). As detailed below, we will show that the degree of structural change (namely, atrophy) within specific dorsal and anterior sections of the thalamus predicts 6-month change in behavioral outcome measures. Our approach differs from virtually all previous studies in two key aspects. First, our longitudinal design allows us to look at the dynamics of thalamic structural change in the first 6 months post-TBI. Second, we focus on individual nuclei within the thalamus, as opposed to considering it as a unitary structure, a degree of resolution that is very important considering that specific regions of the thalamus may play a key role in severe brain injury (Schiff, 2010).

2. Materials and methods

2.1. Patient population

A convenience sample of 25 acute TBI patients (21 male, 4 female; mean age 35.6 years, SD = 15.25) was enrolled in the study (see Table 1 for individual patient demographic, behavioral scores and acute-to-chronic percent brain volume change). Patients were recruited during a time-span of 30 months as part of the UCLA Brain Injury Research Center (BIRC) activity. The main inclusion criterion was an admission Glasgow Coma Scale (GCS; Teasdale and Jennett, 1974) score of ≤8, or an admission GCS of 9–14 with computerized tomography (CT) brain scans demonstrating intracranial bleeding. The main exclusion criteria were GCS >14 with a non-significant head CT, history of neurologic disease or TBI, brain death, and unsuitability to enter the MRI environment (e.g., due to any non MRI-safe implant). Informed written assent was obtained from the patient's legal representative. The study was approved by the UCLA institutional review board. Informed consent was obtained from surrogates as per state regulations.

Table 1
Patient demographics, behavioral scores, acute-to-chronic percent brain volume change (PBVC) and days post-injury at which acute and chronic MRI scans (MRI_A and MRI_C, respectively) were performed.

Pat	Age	Sex	GCS	GOSe	PBVC (%)	MRI_A	MRI_C
1	31	M	9	3	2.18	2	201
2	33	M	12	4	−3.02	3	238
3	20	M	4	4	2.34	12	195
4	25	M	14	8	−0.66	1	200
5	45	M	14	8	−2.3	2	176
6	34	M	7	4	−1.36	4	261
7	62	F	7	3	−2.12	5	194
8	60	M	3	3	−4.06	2	204
9	29	F	14	8	−0.74	12	138
10	64	M	3	2	−7.2	23	199
11	45	M	6	3	−1.2	4	430
12	25	M	14	7	0.15	32	209
13	60	M	14	3	−4.05	3	194
14	23	M	3	8	−1.62	1	162
15	17	M	3	4	−4.63	2	181
16	47	M	12	6	2.06	28	182
17	41	M	3	2	−1.73	1	202
18	18	M	12	4	1.32	10	176
19	34	M	8	3	−4.77	3	186
20	25	F	8	5	−2.65	1	184
21	54	M	3	5	−1.23	24	207
22	40	M	3	5	0.95	2	182
23	16	M	3	3	−7.93	2	194
24	16	M	3	5	2.76	2	196
25	27	F	3	2	−5.7	2	246

2.2. Experimental design

Each patient underwent two structural MRI scans, one shortly after the ictal event (henceforth, “acute”), and one at an approximate 6 month interval (henceforth, “chronic” or “follow-up,” interchangeably). The specific day on which the acute scan occurred depended upon the decision of medical personnel blinded to the aims of this study, and was mainly driven by the patient being stable enough to undergo the session, and general patient safety concerns. (The day of the chronic scan was mainly driven by contingent factors such as patient transportation to the hospital, patient availability, and scheduling.) In addition, patients also underwent two behavioral assessments. An initial GCS assessment was conducted acutely in the emergency room (post-resuscitation), and a Glasgow Outcome Scale extended (GOSe Wilson, 1998) assessment was conducted at follow-up. Acute data acquisition occurred between 1 and 32 days post-injury, with 72% of the patients being scanned within 5 days and the remaining 28% being scanned between 10 and 32 days. The median acute scan occurred on day 3. Follow-up scanning occurred between 138 and 430 days post-injury, with 72% of the patients being scanned before 202 days, and the remaining between 204 and 430 days. The median chronic data acquisition occurred at the 195-day mark. The temporal distance between acute and chronic scans ranged between 126 and 426 days, with 76% of the patients being re-scanned within 200 days from the acute visit, and only the remaining 6 being scanned at a longer interval (between 201 and 426 days). The median inter-scan interval was 183 days.

2.3. MRI data acquisition

T1-weighted MP-RAGE images (TR = 2250 ms, TE = 2.99 ms, FA = 9°, FOV = 256 × 240 × 160 mm, resolution = 1 mm^3 isovoxel) were acquired on a 3 T Siemens Tim Trio scanner at the Ronald Reagan Medical Center at UCLA.

2.4. Data analysis

2.4.1. Tensor-based morphometry. Longitudinal analysis of tissue volume change was performed employing tensor-based morphometry (Thompson et al., 2000). Quantitative maps of longitudinal local tissue compression or expansion were derived from Jacobian maps of the nonlinear image registration of each subject's acute and chronic MRI scans (Hua et al., 2010a, 2011; Leow et al., 2006, 2009; Lu et al., 2011; Thompson et al., 2000). The Jacobian map is the determinant of the Jacobian matrix of a deformation field and encodes the local volume difference between the source and target image (Leow et al., 2007). Jacobian maps were derived in accordance with previous studies (Ashburner et al., 1998, 2003; Fox and Freeborough, 1997; Leow et al., 2005a, 2005b; Studholme et al., 2001; Thompson et al., 2000). First, an initial linear registration was performed to align each subject's follow-up scan to their acute scan (using a 9 degrees of freedom registration; Jenkinson et al., 2002). Second, using the LONI pipeline processing environment (Dinov et al., 2009; Rex et al., 2003), the linearly aligned brains were registered via an intensity-based approach using a high-dimensional, elastic, non-linear algorithm (Leow et al., 2005a, 2005b), an approach considered to be more accurate than feature-based methods (Chen et al., 2003). The registration algorithm employed a mutual information (MI) cost function and the symmetrized Kullback–Leibler (KL) distance as a regularizing term (Hua et al., 2009, 2010a, 2010b; Yanovsky et al., 2008, 2009), a procedure that has been shown to be equivalent to considering both the forward and backward mapping in image registration (Leow et al., 2007). The KL MI procedure is incorporated into a multi-scale bundle that uses multiple grid sizes to compute both regional and local deformations. Our implementation used 300 iterations at 32×32 grid with no iterations at 64×64 because the finer resolution step reduced quality of nonlinear registration and the 32×32 grid captured most of the information for registration. Finally, the determinant of each subject's deformation field (also referred to as the Jacobian matrix) was calculated to obtain a within subject Jacobian map representing regions of tissue expansion or contraction. As suggested by prior literature, we took the natural logarithm of the Jacobian determinant values to decrease unevenness in the range of positive and negative values (Ashburner et al., 1998; Cachier and Rey, 2000; Leow et al., 2005a, 2005b; Woods, 2003).

2.4.2. Percent brain volume change. In order to parcel out the effect of full brain acute-to-chronic volume change on our local analysis of thalamic volume change, we independently estimated two-timepoint percentage brain volume change (PBVC) using SIENA (Smith et al., 2001, 2002), part of the FSL software (Smith et al., 2004). SIENA first extracts brain and skull images from the two-timepoint whole-head input data (Smith, 2002). The two brain images are then aligned to each other using the skull images to constrain the registration scaling (Jenkinson and Smith, 2001; Jenkinson et al., 2002) and resampled into the space halfway between the two. Next, tissue-type segmentation is carried out (Zhang et al., 2001) in order to find brain/non-brain edge points. The perpendicular edge displacement between the two timepoints is then estimated for each edge. Finally, the mean edge displacement is converted into a (global) estimate of percentage brain volume change.

2.4.3. Thalamus parcellation. For each patient, right and left thalami were segmented into 11 structurally defined regions of interest (ROI) on the basis of the ICBM Deep Nuclei Probabilistic Atlas (see Fig. 1; Mazziotta et al., 2001). ROIs included the anterior nucleus (AN), ventral anterior (VAN), ventral lateral (VLN), ventral posteromedial (VPMN), ventral posterolateral (VPLN), dorsomedial (DMN), lateral dorsal (LDN), lateral posterior (LPN), pulvinar (PlvN), medial geniculate (MGN), and lateral geniculate (LGN) nuclei. Individual ICBM thalamic labels were registered to each patient's acute MP-RAGE image, and the corresponding Jacobian map values were averaged within each ROI. To ensure accurate registration of the ICBM thalamic labels to each subjects space, the following 3-step procedure was implemented: (1) Each subject's acute scan was registered to the MNI152 space employing a subcortically tuned algorithm ("first flirt," part of the FSL suite; Jenkinson and Smith, 2001) that uses a subcortical mask for weighting; (2) The MNI152 image was then registered to the ICBM Template image; (3) The two matrices obtained from steps 1 and 2 were concatenated, inverted and applied to the ICBM thalamic labels in order to transform them into individual subject space. All resulting ROIs were visually inspected to ensure registration effectiveness.

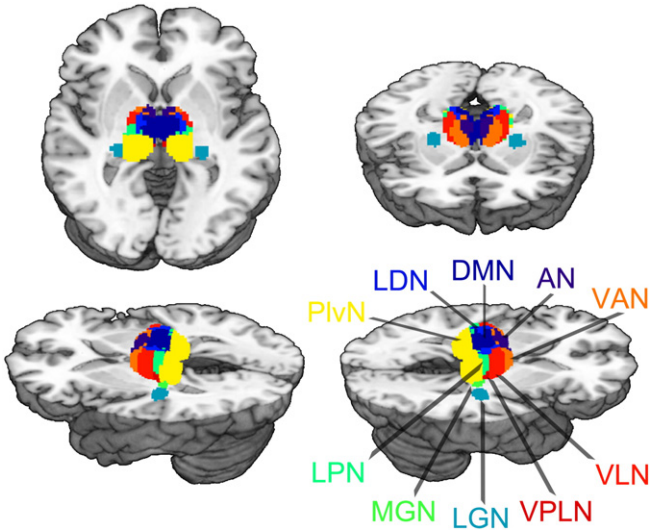

Fig. 1. ROI parcellation of thalamus (ICBM Thalamic Atlas; Mazziotta et al., 2001). Abrv.: AN, anterior nucleus; VAN, ventral anterior nucleus; VLN, ventral lateral nucleus; VPLN, ventral posterolateral nucleus; DMN, dorsomedial; LDN, lateral dorsal nucleus; LPN, lateral posterior nucleus; PlvN, pulvinar nucleus; MGN, medial geniculate nucleus; LGN, lateral geniculate nucleus. (VPMN, ventral posteromedial nucleus, not shown.)

2.4.4. Statistical analysis. TBM scores for each nucleus were analyzed using Stata (version 12, Stata Corp., 2011 College Station, TX, USA). Because 8 of the 11 ROI exhibited non-normal distributions of TBM scores ($p < 0.05$; AN, LDN, VAN, PLN, PMN, MGN), according to a Shapiro–Francia test for normality, and other 2 were marginally non-normal ($p \approx 0.085$; DMN, PlvN) analyses on single nuclei are carried out with non-parametric methods. First, we assessed, for each nucleus independently, whether there was a significant acute-to-chronic TBM change (i.e., atrophy/expansion), using a sign test. Second, we assessed whether the degree of atrophy or expansion within each nucleus (independently) was associated with the six-month GOSe using a Spearman's ρ rank correlation coefficient. In light of the significant correlations between TBM nuclei scores, prior to using thalamic data for regression purposes, all ROIs were entered into a Principal Component Analysis (PCA, with varimax rotation of the loading matrix; Kaiser, 1958). The top 3 components (accounting for 89% of the variance) were retained for further analysis and entered into a robust regression predicting the six-month GOSe together with several covariates including patient age, gender, GCS score, ROI hemisphere laterality, acute-to-chronic PBVC, and days post-injury of each of the acute and chronic scans.

2.4.5. Decision tree induction. Lastly, to characterize the relative importance of demographic, behavioral and physiological data in predicting recovery of consciousness, we entered age, gender, GCS, individual ROI Jacobian data, ROI hemisphere laterality, and acute-to-chronic PBVC in a decision tree model attempting to predict whether a patient had regained consciousness (i.e., $GOSe \geq 3$) by the 6-month assessment or not (i.e., $GOSe = 2$). Decision tree induction and cross-validation was performed using RapidMiner (Mierswa et al., 2006). Classification trees are decision trees derived using recursive data-partitioning algorithms

that classify each observation into one of the class labels for the outcome (in our design: VS or better; cf. Shmueli et al., 2010). Binary classification trees are induced "top–down" by starting with all the data and partitioning it into two subsets (a left and a right daughter node). In turn, each sub-partition (or daughter node) is further split into left and right daughters. The process is repeated recursively until the tree cannot be partitioned further due to lack of data or some stopping criterion is reached (Ishwaran and Rao, 2009). The type of partitioning considered here is univariate in the sense that splits are performed along one unique dimension (i.e., variable). The dimension along which to split the data, at each iteration, is chosen on the basis of so-called "impurity" algorithms, which is to say, algorithms that measure how homogeneous the induced partitions are with respect to the outcome variable. The more homogeneous the observations within each branch of the tree, with respect to the outcome variable, the purer it is, hence the better the partitioning. Here, the variable along which to partition the data at each iteration was thus induced on the basis of an information gain criterion (Quinlan, 1987), an algorithm that uses the concept of entropy to quantify impurity (Rokach and Maimon, 2005). In this setting, entropy can be thought of as the degree of uncertainty concerning whether a given patient falls in the six-month GOSe group. The un-partitioned dataset has the highest level of entropy, since all patients, whether they are VS or better, fall in the same group. The perfectly partitioned dataset, in which all patients with a GOSe of 2 are in one branch of the tree and all other patients are in a different branch, would have the least entropy. At each split, then, information gain is the change (possibly the reduction) in entropy afforded by partitioning the observations into two sub-groups determined by one of the attributes (e.g., GCS scores, or degree of atrophy in an ROI). To avoid over-fitting and to improve generality of the result, we employed pruning and pre-pruning in order to exclude splits with low or non-significant information gain (Fürnkranz, 1997). Assessment of the accuracy of the induced tree was performed using an exhaustive *leave-one-out* k-fold cross-validation, as implemented in Rapid Miner. In this approach, the decision tree is built on the basis of $n-1$ observations, and its accuracy is assessed by testing the induced tree on the nth observation (the one that had been left out). This procedure is repeated by holding out once, in turn, each observation.

3. Results

3.1. Behavioral assessments

Patients' admission GCS score ranged between 3 and 14, with 64% of patients falling in the severe range (i.e., ≤8). The median GCS score was 7 while the mode was 3. At follow-up, GOSe scores ranged between 2 and 8 with a median of 4 and a mode of 3. All patients with a severe acute GCS exhibited 6-month GOSe scores indicating lower moderate disability or worse (i.e., GOSe ≤ 5; cf. Table 1). Of these patients, half were in a vegetative state or lower severe disability state (i.e., GOSe equal to 2 or 3, respectively) at 6-months post-injury. The remaining patients were in a state of upper severe disability or lower moderate disability (i.e., GOSe equal to 4 or 5, respectively). One patient with a severe acute GCS progressed, by 6-months post-injury, to upper good recovery (i.e., GOSe = 8). Of the patients with an acute GCS of 9 or more, 4 were in a severe disability state (evenly split between upper and lower severe disability; i.e., GOSe = 3 or 4, respectively), 4 progressed to make good recovery (evenly split between upper and lower good recovery; i.e., GOSe = 7 or 8, respectively), and 1 patient progressed to a state of upper moderate disability (i.e., GOSe = 6).

3.2. Neuroimaging results

Acute to chronic volume change data for each nucleus are reported in Table 2 and Fig. 2. Collapsing across all patients, several nuclei presented an acute-to-chronic volume change significantly different from zero. Nonetheless, only 4 nuclei were statistically significant after Bonferroni correction for multiple comparisons; namely, the AN and LDN ROIs exhibited severe atrophy over time, while the VPLN and MGN exhibited small, but significant, tissue expansion.

As shown in Fig. 3, however, only for a few ROIs the degree of atrophy was significantly correlated with the six-month outcome. When corrected for multiple comparisons, only one nucleus exhibited a significant association with the six-month GOSe, the AN, which correlated positively with the outcome measure ($\rho = 0.46$, $p < 0.001$). Considering that the TBM values in this nucleus are mostly negative (cf., Table 2 and Fig. 3), this association is best interpreted as implying that the less the atrophy in this nucleus the better the outcome. The DMN and LDN also exhibited the same pattern of association with the outcome measure ($\rho = 0.31$, $p \approx 0.03$, for both ROIs), although neither met family-wise Bonferroni criterion. One ROI exhibited the reverse association (although it did not reach Bonferroni criterion). Namely, the MGN exhibited a significant negative correlation with the six-month GOSe score ($\rho = -0.34$, $p \approx 0.02$). Considering that values in this ROI are mostly positive (cf., Table 2 and Fig. 3), this association is best interpreted as implying that the less the tissue expansion in this region the better the outcome. Finally, the VLPN also exhibited this same pattern of association, but was only marginally significant at the individual test level ($\rho = -0.27$, $p \approx 0.06$), and thus also did not survive family-wise statistical correction.

When all ROIs were entered into a PCA, the data reduction procedure returned 3 components cumulatively accounting for 89% of the total variance. The first component captured the postero-lateral and ventro-lateral aspect of the thalamus, including the LPN, VPLN, VPMN, PlvN and MGN ROIs. The second component grouped anterior and dorsal aspects of the thalamus, encompassing the AN, DMN, LDN, and VAN nuclei. Finally, the last component captured the LGN ROI, as well as the VLN (although this last one contributed almost equally to the first component). The three components were entered in a robust regression to predict the outcome score (GOSe) at 6 months post-injury. In addition, we entered in the regression several covariates: the initial GCS score, age, gender, ROI hemisphere laterality, as well as the acute-to-chronic PBVC to parcel out overall brain atrophy occurring between the two time-points. We also included as covariates the days post-injury at which each scan was performed in order to account for the known association between time and atrophy, and for the across patient variance in the day of examination. The results of the regression indicated that the model was significant ($F(10,39) = 7.64$, $p < 0.001$) and exhibited a good data fit ($R^2 = 0.44$), as computed by the appropriate iteratively re-weighted least squares procedure (see Street et al., 1988). In particular, the second component (namely, the anterior and medial-dorsal ROIs) was significantly related to the six-month outcome measure ($\hat{\beta} = 0.27$, $p = 0.045$) entailing that the less the atrophy in these regions, the higher the chances of a better six-month GOSe. Neither of the remaining thalamic components appeared to be predictive of the outcome measure. The acute-to-chronic PBVC also exhibited a positive relationship with

Table 2
Description of each nucleus' average (M), standard deviation (SD), minimum and maximum acute-to-chronic change. p-Value refers to a sign test assessing whether the average six-month change is significantly different from zero. "**" indicates p ≤ 0.05 Bonferroni corrected.

Nucleus	M	SD	Min	Max	p-Value
AN	−15.26	19.69	−58.94	20.34	<0.001**
LDN	−13.86	15.73	−62.45	10.33	<0.001**
DMN	−6.35	11.14	−34.48	11.72	0.015
VAN	−4.27	10.97	−34.85	18.18	0.015
VLN	0.77	9.16	−25.88	24.95	n.s.
VPMN	2.97	6.41	−9.28	26.34	0.033
VPLN	3.76	7.90	−13.01	31.34	<0.001**
LPN	−3.64	10.01	−37.68	21.56	0.033
LGN	2.00	11.18	−24.93	33.68	n.s.
MGN	5.31	8.91	−14.24	38.57	0.003**
PlvN	−2.24	8.54	−28.74	19.32	n.s.

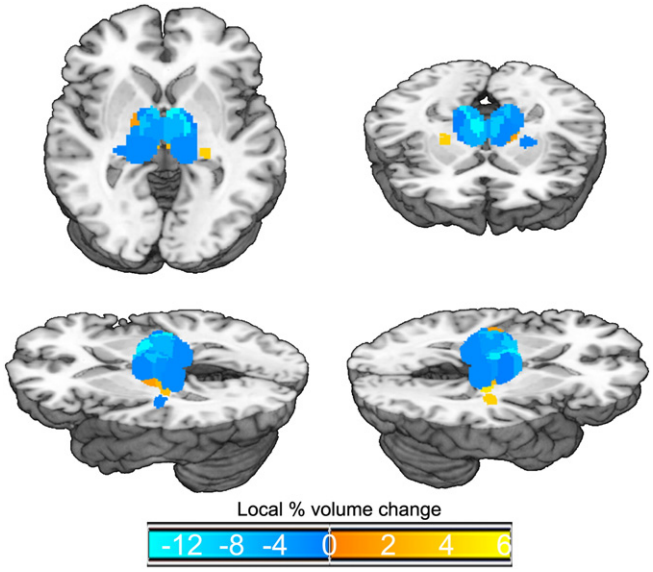

Fig. 2. Average TBM values for each thalamic nucleus across all patients. Cold colors mark regions of tissue atrophy, warm colors mark regions of tissue expansion. Brighter colors indicate regions presenting greater volume change. (This visualization was obtained by assigning to each of the ROIs shown in Fig. 1 the average TBM value across patients; and not by transforming individual patient data into a common template.)

the follow-up outcome measure ($\hat{\beta} = 0.17$, $p = 0.014$). Considering that PBVC is mostly negative (cf. Table 1), this relationship is best interpreted as indicating that the less the acute-to-chronic atrophy, the better the chances of a higher 6-month GOSe. Two other covariates appeared to be significantly related to the six-month GOSe score: post-resuscitation GCS ($\hat{\beta} = 0.09$, $p = 0.029$) and age ($\hat{\beta} = -0.03$, $p = 0.013$). As expected, the former measure correlated positively with the six-month outcome, entailing that a less severe GCS score was indicative of a better outcome, whereas the latter correlated negatively, indicating that the older the patient the worse the GOSe measure. Finally, we note that although only marginally, the days post-injury of the acute scan also correlated positively with the follow-up GOSe ($\hat{\beta} = 0.04$, $p = 0.058$). This positive marginal association demonstrates that it was important to include the temporal variables in the analysis. Nonetheless, it is difficult to interpret an association according to which the later a patient underwent the acute MRI scan, the better the behavioral outcome measure. This marginal association might thus be spurious, or reflect some other factor which might have had itself an association with the choice of day of scanning (which, as stated in the Materials and methods section, was decided independently by medical personnel blind to the aims of this study). At present we cannot distinguish between the two possibilities.

The binary decision tree induced over the data is depicted in Fig. 4. Overall, the decision tree achieved 84% accuracy in differentiating patients who remained in a VS at six months (i.e., GOSe of 2) versus patients who regained consciousness. As shown in the figure, two attributes including physiological and behavioral measures formed the basis of the decision tree: volume change in the anterior nucleus ROIs and the post-resuscitation GCS score. The TBM measurement in the AN was the most important attribute, itself separating patients into two groups (approximately 61% and 39% for the left and right branches, respectively) according to whether they exhibited extreme atrophy in this ROI (with threshold value of −16.74%). Patients who did not exhibit extreme atrophy in the AN all regained consciousness, exhibiting a score of 3 or more in the 6-month GOSe. Of the patients who exhibited extreme atrophy in the AN, those with a post-resuscitation GCS of at least 5 also regained consciousness. Of the patients who exhibited extreme atrophy in the AN and an initial GCS of 4 or less, 80% failed to regain consciousness, while 20% did. In other words, all patients who failed to regain consciousness presented extreme atrophy in the AN and an initial GCS of 4 or less. There was, however, a small fraction of patients with this same neurophysiological and behavioral profile who did regain consciousness. Further research and larger samples will have to address which factor(s) might have contributed to this small uncertainty. Taken together, this multivariate and data driven methodology is in good agreement with the hypothesis-driven analysis described

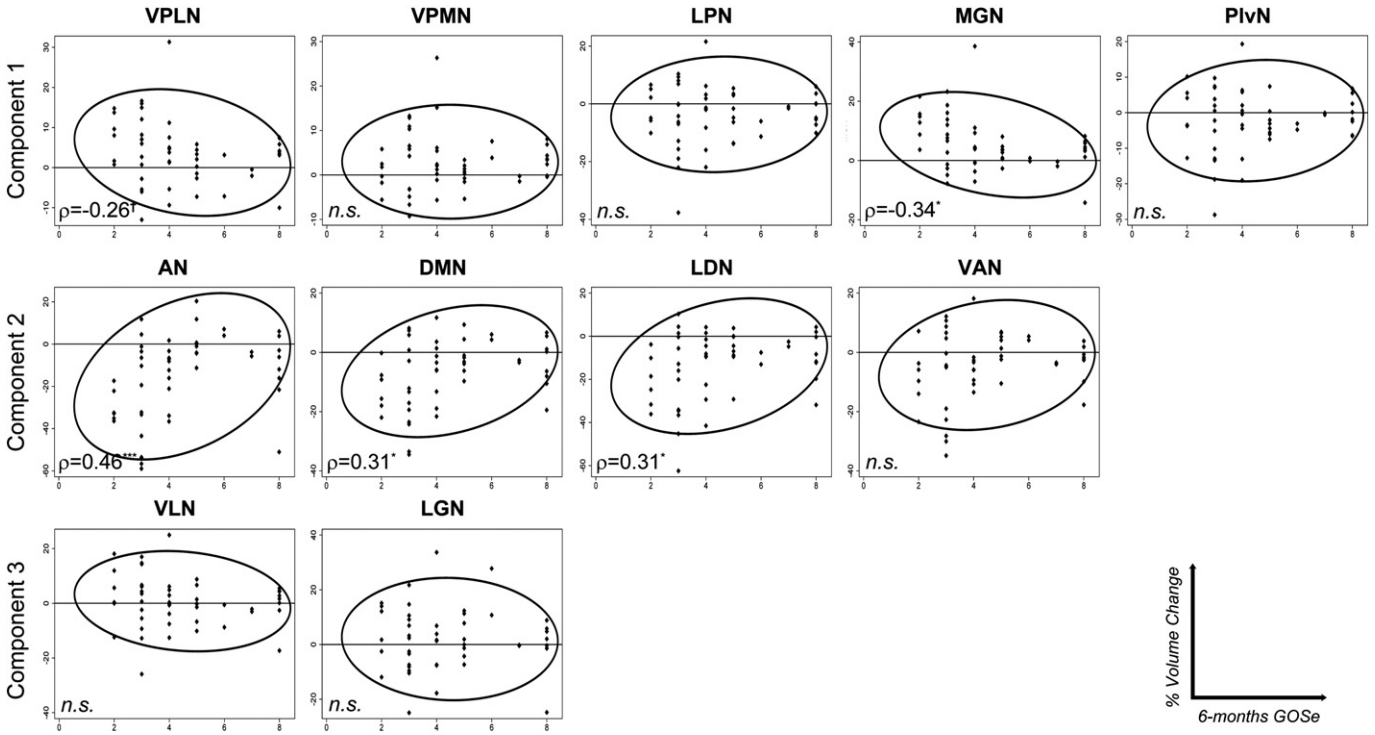

Fig. 3. Scatterplots depicting the distribution of ROI tensor-based morphometry values as a function of the six-month GOS (with confidence ellipsis). Spearman's rank correlation coefficient 'ρ' is reported, for each variable; '***' indicates $p < 0.001$; '*' indicates $0.05 \leq p \leq 0.01$; '†' indicates $p = 0.06$; '*n.s.*' indicates not significant.

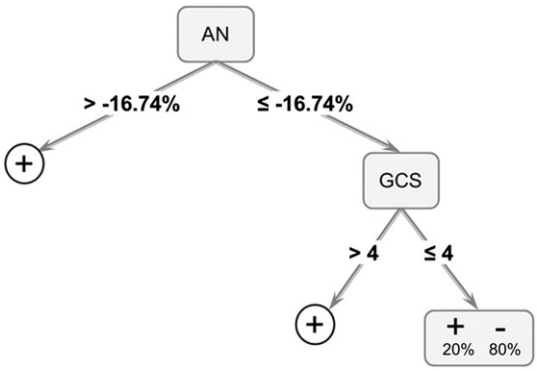

Fig. 4. Binary decision tree classifying patients who did not regain consciousness (i.e., 6-month GOSe of 2; "−") versus patients who did regain consciousness (6-month GOSe ≥ 3;"+"). (AN, anterior nucleus; GCS, Glasgow Coma Scale).

above, and provides a (preliminary) flow-chart integrating and ranking the importance (in our data) of behavioral and quantitative physiological metrics of brain change. This highlights the relative predictive power of the collected variables and suggests the power of pooling together multiple sources of information.

4. Discussion

In this report, we have examined the relation between acute-to-chronic structural change within the subregions of the thalamus and behavioral change in a group of moderate to severe TBI patients. As reported in previous research, thalamus is significantly affected by TBI on a global basis (Adams et al., 2000; Babikian et al., 2005; Fearing et al., 2008). Our nucleus-wise analysis, however, allowed us to isolate different patterns of structural change. Specifically, we find that the antero-dorso-medial aspect of the thalamus is the target of localized tissue atrophy, consistent with the finding that these same regions appear to be particularly atrophied in chronic vegetative state and minimally conscious state patients (Fernández-Espejo et al., 2010), and with a recent proposal discussing the crucial role of the thalamus in the recovery of awareness and cognitive function after severe brain injury (Schiff, 2010). Our data therefore support the view that, perhaps because of their connectivity geometry, some aspects of the thalamus are crucial to sustaining functional integration through long-range cortico-cortical pathways as well as cortico-striatopallidal-thalamocortical loop connections (Schiff, 2008). Indeed, there is a remarkable overlap between the regions known to be directly interconnected with the antero-dorso-medial aspect in the thalamus and medial and lateral prefrontal cortices which, when metabolically dysfunctional, are considered to be the hallmark of chronic vegetative states after severe brain injury (Laureys, 2005). Consistent with this view, the thalamo-frontal connectivity has been reported to be restored upon recovery of a patient's behavioral responsiveness after protracted unconsciousness (Laureys et al., 2000), and some pharmacologic interventions have been shown to induce behavioral ameliorations concurrently with a restoration of frontal metabolism (Brefel-Courbon et al., 2007). Similarly, the successful increase in behavioral responsiveness of some patients with impairments of consciousness after deep brain stimulation to the (central) thalamus (Schiff et al., 2007) has been interpreted as following a functional restoration of thalamo-cortical circuits (Schiff, 2008, 2010).

The anterior nucleus, which is encased between the arms of the rostral segments of the internal medullary lamina is reciprocally connected with the limbic cortex including the anterior cingulate gyrus, retrosplenial area and pre- and para-subiculum (Kaitz and Robertson, 1981; Robertson and Kaitz, 1981). This region is believed to play an important role in learning and memory (Gabriel et al., 1983) since lesions in this area are known to impair mnestic functions (inducing diencephalic amnesia; Van der Werf et al., 2003), possibly through a disruption of neural plasticity processes in distal limbic brain regions (Dumont et al., 2012). In particular, damage to this region induces severe anterograde and temporally graded retrograde amnesia, along with impaired subjective memory, resembling patients with hippocampal system injury (Hampstead and Koffler, 2009). Furthermore, lesions in this region have also been associated with impaired regulation of affective responses to environmental conditions, through its connection with medial prefrontal limbic regions (Dupire et al., 2013). From a connectivity as well as a structural point of view, the lateral dorsal nucleus, which is also encased within the two rostral arms of the internal medullary lamina, is very similar to the anterior nuclei (van Groen et al., 2002), although the projections from the entorhinal cortex, presubiculum and parasubiculum to the lateral dorsal nucleus might be denser (Saunders et al., 2005). Sharing its connection geometry with the anterior nucleus, the lateral dorsal nucleus is also considered to be part of the thalamo-hippocampal system, and therefore important for recollection (Cipolotti et al., 2008). Overall, these two nuclei appear to be the major thalamic recipients of projections from limbic cortex (Kaitz and Robertson, 1981). The dorsomedial nucleus, which is particularly large in humans (Nieuwenhuys et al., 2008), represents the main subcortical structure that projects to the prefrontal cortex (PFC), and is reciprocally connected with lateral orbitofrontal, medial frontal/cingulate, and lateral prefrontal cortex (Klein et al., 2010). From a functional point of view, this nucleus is believed to play a key role in regulating the cognitive functions of prefrontal cortex (Rotaru et al., 2005), and to therefore participate, perhaps mostly through its connection to dorsolateral prefrontal cortex, in higher cognitive functions (Watanabe and Funahashi, 2004) including various types of memory and the construction of prospective information (Watanabe and Funahashi, 2012) as well as executive functioning (Van der Werf et al., 2003). Furthermore, the DMN has also been involved in aspects of consciousness because of its role (together with the intra-laminar group) in the generation of absence seizure-like episodes in rodents (Banerjee and Snead, 1994; Kato et al., 2008). The ventral anterior nucleus is reciprocally connected with the premotor sections of frontal cortex, including the frontal eye fields (Brodmann area 8) and the supplementary motor area (SMA), as well as prefrontal cortex, and particularly the anterior cingulate gyrus. In addition, this nucleus also receives afferent connections from the substantia nigra pars compacta and the globus pallidus pars medialis, completing a cortico-subcortical circuit crucial for motor planning (Nieuwenhuys et al., 2008).

Overall, we find that different classes of thalamic nuclei (Nieuwenhuys et al., 2008) are affected by severe traumatic brain injury, and that the degree of atrophy in a specific subset of thalamic nuclei is correlated with a patient's behavioral outcome at six months post-injury. On the one hand, association nuclei (i.e., DMN) and limbic nuclei (i.e., AN, LDN) were the site of tissue atrophy, and exhibited increased atrophy in patients with poor six-month behavioral outcome. On the other hand, we find that two sensory nuclei (i.e., MGN and VPLN) underwent little, but systematic, tissue expansion over the first six months post-injury. Their association with the behavioral outcome, however, was not very strong (neither survived Bonferroni criterion, and the VPLN correlated only marginally with the GOSe when individually tested; $p = 0.06$ — see the Results section). Consistent with this pattern, the principal component in which both nuclei were included was not significantly related to the outcome measure either. Nonetheless, thalamic expansion following brain injury has been reported previously in conjunction with acute and secondary delayed processes triggered by brain injury (Osteen et al., 2001; Pierce et al., 1998). In particular, the medial geniculate nucleus and the ventro-posterior aspect (among others) of the rodent thalamus were found to be enlarged due to calcium accumulation reflecting secondary cell death (Osteen et al., 2001). While previous studies have also shown that pathologies such as necrotic neurons, macrophages, reactive astrocytes and cellular debris, can selectively affect individual nuclei (Bramlett et al., 1997), at present we can only speculate about the importance of the specific cytoarchitectonics of each nucleus

in determining the dynamic cascade of neural events triggered by severe brain injury.

As discussed above, the nuclei exhibiting severe atrophy receive afferent connections and project efferent fibers mainly to medial limbic, and medial and lateral prefrontal cortices, regions at the heart of several cognitive functions spanning memory, executive functions, and awareness — capacities central to a normal brain and the disruption of which is consistent with very low performance on a GOSe assessment (although the mediating factor of motor impairments, which might be associated with VAN atrophy, cannot be discounted here; cf. Bekinschtein et al., 2008).

Finally, it is worth closing with a note of caution concerning some limitations of the present study. First, while we have adopted the widely employed "nuclear" view of the thalamus, this approach is not uncontroversial (see Sherman and Guillery, 2001 for discussion). Specifically, it does not account for the fact that each individual nucleus or nuclear subdivision can host a variety of intermingled relay cell types which might be differently susceptible to brain injury. Similarly, our approach is also blind to the fact that thalamic nuclei are likely to differ in both extrinsic connectivity (e.g., different laminar organization of thalamocortical projections; cf., Herkenham, 1980) as well as intrinsic organization (e.g., distribution of different excitatory and inhibitory metabotropic receptors), a set of differences which might bear some explanatory power relevant to the uneven role of different nuclei in cognitive recovery after TBI. Second, it is not possible for us to differentiate among different modes of firing of thalamic cells (i.e., in tonic versus burst mode), a characteristic of thalamic neurons that is likely to play a key role in its function. Finally, we stress that our findings are bound by the specific methodological choices. On the one hand, we are bound by the structural atlas we chose which, although based on an extremely large number of individual datasets, does not allow us to evaluate some specific subregions of the thalamus, such as the anterior and posterior intralaminar nuclei, which have been proposed to be central to recovery after TBI (by visual inspection these nuclei appear to be included within the AN and DMN ROIs; Schiff, 2008). Furthermore, even though the use of an atlas based on a large population is likely to properly label ROIs, on average, this approach is necessarily introducing greater variance than if we had defined ROIs on the basis of more detailed individual neuroanatomical images (which were not available in this setting). On the other hand, we are also bound, with respect to the precision of our measurement, by the use of the GOSe scale, which although very fitting in this setting, does not have the fine-grained resolution afforded by other scales often employed in severe TBI (e.g., Coma Recovery Scale — Revised; Giacino et al., 2004).

In sum, our findings address secondary processes following severe brain injury, and in particular structural changes across different thalamic nuclei. According to our data, substantial secondary non-mechanical damage triggered by severe trauma occurs well after the first week post-injury (although we cannot tell at which point within our two-timepoint sampling), suggesting a temporal window within which intervention might be possible. Furthermore, our results suggest a clear role for specific subregions of the thalamus within its anterior and medio-dorsal aspects in TBI outcome, consistent with the view that these specific sections of the thalamus are crucial to awareness and to maintaining neuronal firing patterns across long-range cortico-cortical as well as cortico-subcortical loops crucial to global network activity and recovery post severe brain injury (Schiff, 2008, 2010).

References

Adams, J.H., Graham, D.I., Jennett, B., 2000. The neuropathology of the vegetative state after an acute brain insult. Brain 123 (Pt 7), 1327–1338.

Ashburner, J., Friston, K.J., 2000. Voxel-based morphometry—the methods. Neuroimage 11 (6 Pt 1), 805–821.

Ashburner, J., Hutton, C., Frackowiak, R., Johnsrude, I., Price, C., Friston, K., 1998. Identifying global anatomical differences: deformation-based morphometry. Hum. Brain Mapp. 6 (5–6), 348–357.

Ashburner, J., Csernansky, J.G., Davatzikos, C., Fox, N.C., Frisoni, G.B., Thompson, P.M., 2003. Computer-assisted imaging to assess brain structure in healthy and diseased brains. Lancet Neurol. 2 (2), 79–88.

Babikian, T., Freier, M.C., Tong, K.A., Nickerson, J.P., Wall, C.J., Holshouser, B.A., Burley, T., Riggs, M.L., Ashwal, S., 2005. Susceptibility weighted imaging: neuropsychologic outcome and pediatric head injury. Pediatr. Neurol. 33 (3), 184–194.

Banerjee, P.K., Snead III, O.C., 1994. Thalamic mediodorsal and intralaminar nuclear lesions disrupt the generation of experimentally induced generalized absence-like seizures in rats. Epilepsy Res. 17 (3), 193–205.

Bekinschtein, T.A., Coleman, M.R., Niklison, J., Pickard, J.D., Manes, F.F., 2008. Can electromyography objectively detect voluntary movement in disorders of consciousness? J. Neurol. Neurosurg. Psychiatry 79 (7), 826–828.

Boly, M., Tshibanda, L., Vanhaudenhuyse, A., Noirhomme, Q., Schnakers, C., Ledoux, D., Boveroux, P., Garweg, C., Lambermont, B., Phillips, C., Luxen, A., Moonen, G., Bassetti, C., Maquet, P., Laureys, S., 2009. Functional connectivity in the default network during resting state is preserved in a vegetative but not in a brain dead patient. Hum. Brain Mapp. 30 (8), 2393–2400.

Bramlett, H.M., Dietrich, W.D., Green, E.J., Busto, R., 1997. Chronic histopathological consequences of fluid-percussion brain injury in rats: effects of post-traumatic hypothermia. Acta Neuropathol. 93 (2), 190–199.

Brefel-Courbon, C., Payoux, P., Ory, F., Sommet, A., Slaoui, T., Raboyeau, G., Lemesle, B., Puel, M., Montastruc, J.L., Demonet, J.F., Cardebat, D., 2007. Clinical and imaging evidence of zolpidem effect in hypoxic encephalopathy. Ann. Neurol. 62 (1), 102–105.

Cachier, P., Rey, D., 2000. Symmetrization of the non-rigid registration problem using inversion-invariant energies: application to multiple sclerosis. Medical Image Computing and Computer-Assisted Intervention–MICCAI 2000. Springer, pp. 472–481.

Chen, H.M., Chung, A.C., Yu, S.C., Norbash, A., Wells, W., 2003. Multi-modal image registration by minimizing Kullback–Leibler distance between expected and observed joint class histograms. Computer Vision and Pattern Recognition, 2003. Proceedings. 2003 IEEE Computer Society Conference. IEEE, vol. 2, p. II, 570–576.

Christman, C.W., Grady, M.S., Walker, S.A., Holloway, K.L., Povlishock, J.T., 1994. Ultrastructural studies of diffuse axonal injury in humans. J. Neurotrauma 11 (2), 173–186.

Chung, M.K., Worsley, K.J., Paus, T., Cherif, C., Collins, D.L., Giedd, J.N., Rapoport, J.L., Evans, A.C., 2001. A unified statistical approach to deformation-based morphometry. Neuroimage 14 (3), 595–606.

Chung, M.K., Worsley, K.J., Robbins, S., Paus, T., Taylor, J., Giedd, J.N., Rapoport, J.L., Evans, A.C., 2003. Deformation-based surface morphometry applied to gray matter deformation. Neuroimage 18 (2), 198–213.

Cipolotti, L., Husain, M., Crinion, J., Bird, C.M., Khan, S.S., Losseff, N., Howard, R.S., Leff, A.P., 2008. The role of the thalamus in amnesia: a tractography, high-resolution MRI and neuropsychological study. Neuropsychologia 46 (11), 2745–2758.

Coronado, V.G., Xu, L., Basavaraju, S.V., McGuire, L.C., Wald, M.M., Faul, M.D., Guzman, B.R., Hemphill, J.D., 2011. C.f.D.C., (CDC), P. Surveillance for traumatic brain injury-related deaths—United States, 1997–2007. MMWR Surveill. Summ. 60 (5), 1–32.

Dinov, I.D., Van Horn, J.D., Lozev, K.M., Magsipoc, R., Petrosyan, P., Liu, Z., Mackenzie-Graham, A., Eggert, P., Parker, D.S., Toga, A.W., 2009. Efficient, distributed and interactive neuroimaging data analysis using the LONI pipeline. Front. Neuroinform. 3, 22.

Dumont, J.R., Amin, E., Poirier, G.L., Albasser, M.M., Aggleton, J.P., 2012. Anterior thalamic nuclei lesions in rats disrupt markers of neural plasticity in distal limbic brain regions. Neuroscience 224, 81–101.

Dupire, A., Kant, P., Mons, N., Marchand, A.R., Coutureau, E., Dalrymple-Alford, J., Wolff, M., 2013. A role for anterior thalamic nuclei in affective cognition: interaction with environmental conditions. Hippocampus 23 (5), 392–404.

Fearing, M.A., Bigler, E.D., Wilde, E.A., Johnson, J.L., Hunter, J.V., Li, Xiaoqi, Hanten, G., Levin, H.S., 2008. Morphometric MRI findings in the thalamus and brainstem in children after moderate to severe traumatic brain injury. J. Child Neurol. 23 (7), 729–737.

Fernández-Espejo, D., Junque, C., Bernabeu, M., Roig-Rovira, T., Vendrell, P., Mercader, J., 2010. Reductions of thalamic volume and regional shape changes in the vegetative and the minimally conscious states. J. Neurotrauma 27 (7), 1187–1193.

Fox, N.C., Freeborough, P.A., 1997. Brain atrophy progression measured from registered serial MRI: validation and application to Alzheimer's disease. J. Magn. Reson. Imaging 7 (6), 1069–1075.

Fox, N.C., Warrington, E.K., Freeborough, P.A., Hartikainen, P., Kennedy, A.M., Stevens, J.M., Rossor, M.N., 1996. Presymptomatic hippocampal atrophy in Alzheimer's disease. A longitudinal MRI study. Brain 119 (Pt 6), 2001–2007.

Fox, N.C., Scahill, R.I., Crum, W.R., Rossor, M.N., 1999. Correlation between rates of brain atrophy and cognitive decline in AD. Neurology 52 (8), 1687–1689.

Fox, N.C., Cousens, S., Scahill, R., Harvey, R.J., Rossor, M.N., 2000. Using serial registered brain magnetic resonance imaging to measure disease progression in Alzheimer disease: power calculations and estimates of sample size to detect treatment effects. Arch. Neurol. 57 (3), 339–344.

Fox, N.C., Crum, W.R., Scahill, R.I., Stevens, J.M., Janssen, J.C., Rossor, M.N., 2001. Imaging of onset and progression of Alzheimer's disease with voxel-compression mapping of serial magnetic resonance images. Lancet 358 (9277), 201–205.

Freeborough, P.A., Fox, N.C., 1997. The boundary shift integral: an accurate and robust measure of cerebral volume changes from registered repeat MRI. IEEE Trans. Med. Imaging 16 (5), 623–629.

Freeborough, P.A., Woods, R.P., Fox, N.C., 1996. Accurate registration of serial 3D MR brain images and its application to visualizing change in neurodegenerative disorders. J. Comput. Assist. Tomogr. 20 (6), 1012–1022.

Fürnkranz, J., 1997. Pruning algorithms for rule learning. Mach. Learn. 27 (2), 139–171.

Gabriel, M., Lambert, R.W., Foster, K., Orona, E., Sparenborg, S., Maiorca, R.R., 1983. Anterior thalamic lesions and neuronal activity in the cingulate and retrosplenial cortices during discriminative avoidance behavior in rabbits. Behav. Neurosci. 97 (5), 675–696.

Ge, Y., Grossman, R.I., Udupa, J.K., Wei, L., Mannon, L.J., Polansky, M., Kolson, D.L., 2000. Brain atrophy in relapsing–remitting multiple sclerosis and secondary progressive multiple sclerosis: longitudinal quantitative analysis. Radiology 214 (3), 665–670.

Giacino, J.T., Kalmar, K., Whyte, J., 2004. The JFK Coma Recovery Scale-Revised: measurement characteristics and diagnostic utility. Arch. Phys. Med. Rehabil. 85 (12), 2020–2029.

Hall, E.D., Sullivan, P.G., Gibson, T.R., Pavel, K.M., Thompson, B.M., Scheff, S.W., 2005. Spatial and temporal characteristics of neurodegeneration after controlled cortical impact in mice: more than a focal brain injury. J. Neurotrauma 22 (2), 252–265.

Hampstead, B.M., Koffler, S.P., 2009. Thalamic contributions to anterograde, retrograde, and implicit memory: a case study. Clin. Neuropsychol. 23 (7), 1232–1249.

Herkenham, M., 1980. Laminar organization of thalamic projections to the rat neocortex. Science 207 (4430), 532–535.

Hua, X., Leow, A.D., Levitt, J.G., Caplan, R., Thompson, P.M., Toga, A.W., 2009. Detecting brain growth patterns in normal children using tensor-based morphometry. Hum. Brain Mapp. 30 (1), 209–219.

Hua, X., Hibar, D.P., Lee, S., Toga, A.W., Jack Jr., C.R., Weiner, M.W., Thompson, P.M., A.D.N.I., 2010a. Sex and age differences in atrophic rates: an ADNI study with n = 1368 MRI scans. Neurobiol. Aging 31 (8), 1463–1480.

Hua, X., Lee, S., Hibar, D.P., Yanovsky, I., Leow, A.D., Toga, A.W., Jack Jr., C.R., Bernstein, M.A., Reiman, E.M., Harvey, D.J., Kornak, J., Schuff, N., Alexander, G.E., Weiner, M.W., Thompson, P.M., A.D.N.I., 2010b. Mapping Alzheimer's disease progression in 1309 MRI scans: power estimates for different inter-scan intervals. Neuroimage 51 (1), 63–75.

Hua, X., Gutman, B., Boyle, C.P., Rajagopalan, P., Leow, A.D., Yanovsky, I., Kumar, A.R., Toga, A.W., Jack Jr., C.R., Schuff, N., Alexander, G.E., Chen, K., Reiman, E.M., Weiner, M.W., Thompson, P.M., A.D.N.I., 2011. Accurate measurement of brain changes in longitudinal MRI scans using tensor-based morphometry. Neuroimage 57 (1), 5–14.

Ishwaran, H., Rao, J.S., 2009. Decision tree: introduction. In: Kattan, M.W., Cowen, M.E. (Eds.), Encyclopedia of Medical Decision Making. SAGE Publications, Thousand Oaks, CA, pp. 323–328.

Jenkinson, M., Smith, M., 2001. A global optimisation method for robust affine registration of brain images. Med. Image Anal. 5, 143–156.

Jenkinson, M., Bannister, P.R., Brady, J.M., Smith, S.M., 2002. Improved optimisation for the robust and accurate linear registration and motion correction of brain images. Neuroimage 17, 825–841.

Kaiser, H.F., 1958. The varimax criterion for analytic rotation in factor analysis. Psychometrika 23, 187–200.

Kaitz, S.S., Robertson, R.T., 1981. Thalamic connections with limbic cortex. II. Corticothalamic projections. J. Comp. Neurol. 195 (3), 527–545.

Kang, E.K., Kim, D.Y., Paik, N.J., 2012. Transcranial direct current stimulation of the left prefrontal cortex improves attention in patients with traumatic brain injury: a pilot study. J. Rehabil. Med. 44 (4), 346–350.

Kato, K., Urino, T., Hori, T., Tsuda, H., Yoshida, K., Hashizume, K., Tanaka, T., 2008. Experimental petit mal-like seizure induced by microinjection of kainic acid into the unilateral mediodorsal nucleus of the thalamus. Neurol. Med. Chir. (Tokyo) 48 (7), 285–290 (discussion 290–1).

Klein, J.C., Rushworth, M.F.S., Behrens, T.E.J., Mackay, C.E., de Crespigny, A.J., D'Arceuil, H., Johansen-Berg, H., 2010. Topography of connections between human prefrontal cortex and mediodorsal thalamus studied with diffusion tractography. Neuroimage 51 (2), 555–564.

Laureys, S., 2005. The neural correlate of (un)awareness: lessons from the vegetative state. Trends Cogn. Sci. 9 (12), 556–559.

Laureys, S., Faymonville, M.E., Luxen, A., Lamy, M., Franck, G., Maquet, P., 2000. Restoration of thalamocortical connectivity after recovery from persistent vegetative state. Lancet 355 (9217), 1790–1791.

Lemieux, L., Wieshmann, U.C., Moran, N.F., Fish, D.R., Shorvon, S.D., 1998. The detection and significance of subtle changes in mixed-signal brain lesions by serial MRI scan matching and spatial normalization. Med. Image Anal. 2 (3), 227–242.

Leow, A., Huang, S.C., Geng, A., Becker, J., Davis, S., Toga, A., Thompson, P., 2005a. Inverse consistent mapping in 3D deformable image registration: its construction and statistical properties. Inf. Process. Med. Imaging 19, 493–503.

Leow, A., Yu, C.L., Lee, S.J., Huang, S.C., Protas, H., Nicolson, R., Hayashi, K.M., Toga, A.W., Thompson, P.M., 2005b. Brain structural mapping using a novel hybrid implicit/explicit framework based on the level-set method. Neuroimage 24 (3), 910–927.

Leow, A.D., Klunder, A.D., Jack Jr., C.R., Toga, A.W., Dale, A.M., Bernstein, M.A., Britson, P.J., Gunter, J.L., Ward, C.P., Whitwell, J.L., Borowski, B.J., Fleisher, A.S., Fox, N.C., Harvey, D., Kornak, J., Schuff, N., Studholme, C., Alexander, G.E., Weiner, M.W., Thompson, P.M., Study, A.P.P., 2006. Longitudinal stability of MRI for mapping brain change using tensor-based morphometry. Neuroimage 31 (2), 627–640.

Leow, A.D., Yanovsky, I., Chiang, M.C., Lee, A.D., Klunder, A.D., Lu, A., Becker, J.T., Davis, S.W., Toga, A.W., Thompson, P.M., 2007. Statistical properties of Jacobian maps and the realization of unbiased large-deformation nonlinear image registration. IEEE Trans. Med. Imaging 26 (6), 822–832.

Leow, A.D., Yanovsky, I., Parikshak, N., Hua, X., Lee, S., Toga, A.W., Jack Jr., C.R., Bernstein, M.A., Britson, P.J., Gunter, J.L., Ward, C.P., Borowski, B., Shaw, L.M., Trojanowski, J.Q., Fleisher, A.S., Harvey, D., Kornak, J., Schuff, N., Alexander, G.E., Weiner, M.W., Thompson, P.M., A.D.N.I., 2009. Alzheimer's disease neuroimaging initiative: a one-year follow up study using tensor-based morphometry correlating degenerative rates, biomarkers and cognition. Neuroimage 45 (3), 645–655.

Lu, P.H., Thompson, P.M., Leow, A., Lee, G.J., Lee, A., Yanovsky, I., Parikshak, N., Khoo, T., Wu, S., Geschwind, D., Bartzokis, G., 2011. Apolipoprotein e genotype is associated with temporal and hippocampal atrophy rates in healthy elderly adults: a tensor-based morphometry study. J. Alzheimers Dis. 23 (3), 433–442.

MacKenzie, E.J., 2000. Epidemiology of injuries: current trends and future challenges. Epidemiol. Rev. 22 (1), 112–119.

Martin, L.J., Kaiser, A., Yu, J.W., Natale, J.E., Al-Abdulla, N.A., 2001. Injury-induced apoptosis of neurons in adult brain is mediated by p53-dependent and p53-independent pathways and requires bax. J. Comp. Neurol. 433 (3), 299–311.

Mazziotta, J., Toga, A., Evans, A., Fox, P., Lancaster, J., Zilles, K., Woods, R., Paus, T., Simpson, G., Pike, B., Holmes, C., Collins, L., Thompson, P., MacDonald, D., Iacoboni, M., Schormann, T., Amunts, K., Palomero-Gallagher, N., Geyer, S., Parsons, L., Narr, K., Kabani, N., Le Goualher, G., Boomsma, D., Cannon, T., Kawashima, R., Mazoyer, B., 2001. A probabilistic atlas and reference system for the human brain: International Consortium for Brain Mapping (ICBM). Philos. Trans. R. Soc. Lond. B Biol. Sci. 356 (1412), 1293–1322.

Mierswa, I., Wurst, M., Klinkenberg, R., Scholz, M., Euler, T., 2006. YALE: rapid prototyping for complex data mining tasks. In: Ungar, L., Craven, M., Gunopulos, D., Eliassi-Rad, T. (Eds.), KDD '06: Proceedings of the 12th ACM SIGKDD International Conference on Knowledge Discovery and Data Mining. ACM, New York, NY, USA, pp. 935–940.

Monti, M.M., 2012. Cognition in the vegetative state. Annu. Rev. Clin. Psychol. 8, 431–454.

Murray, C.J., Lopez, A.D., 1997. Global mortality, disability, and the contribution of risk factors: global burden of disease study. Lancet 349 (9063), 1436–1442.

Natale, J.E., Cheng, Y., Martin, L.J., 2002. Thalamic neuron apoptosis emerges rapidly after cortical damage in immature mice. Neuroscience 112 (3), 665–676.

Nieuwenhuys, R., Voogd, J., van Huijzen, C., 2008. The Human Central Nervous System, 4th ed. Springer.

O'Brien, J.T., Paling, S., Barber, R., Williams, E.D., Ballard, C., McKeith, I.G., Gholkar, A., Crum, W.R., Rossor, M.N., Fox, N.C., 2001. Progressive brain atrophy on serial MRI in dementia with Lewy bodies, AD, and vascular dementia. Neurology 56 (10), 1386–1388.

Osteen, C.L., Moore, A.H., Prins, M.L., Hovda, D.A., 2001. Age-dependency of 45calcium accumulation following lateral fluid percussion: acute and delayed patterns. J. Neurotrauma 18 (2), 141–162.

Pierce, J.E., Smith, D.H., Trojanowski, J.Q., McIntosh, T.K., 1998. Enduring cognitive, neurobehavioral and histopathological changes persist for up to one year following severe experimental brain injury in rats. Neuroscience 87 (2), 359–369.

Povlishock, J.T., Katz, D.I., 2005. Update of neuropathology and neurological recovery after traumatic brain injury. J. Head Trauma Rehabil. 20 (1), 76–94.

Quinlan, J.R., 1987. Simplifying decision trees. Int. J. Man Mach. Stud. 27 (3), 221–234.

Rex, D.E., Ma, J.Q., Toga, A.W., 2003. The LONI pipeline processing environment. Neuroimage 19 (3), 1033–1048.

Rey, D., Subsol, G., Delingette, H., Ayache, N., 2002. Automatic detection and segmentation of evolving processes in 3D medical images: application to multiple sclerosis. Med. Image Anal. 6 (2), 163–179.

Robertson, R.T., Kaitz, S.S., 1981. Thalamic connections with limbic cortex. I. Thalamocortical projections. J. Comp. Neurol. 195 (3), 501–525.

Rokach, L., Maimon, O., 2005. Top–down induction of decision trees classifiers—a survey. IEEE Trans. Syst. Man Cybern. Part C Appl. Rev. 35 (4), 476–487.

Rotaru, D.C., Barrionuevo, G., Sesack, S.R., 2005. Mediodorsal thalamic afferents to layer iii of the rat prefrontal cortex: synaptic relationships to subclasses of interneurons. J. Comp. Neurol. 490 (3), 220–238.

Saunders, R.C., Mishkin, M., Aggleton, J.P., 2005. Projections from the entorhinal cortex, perirhinal cortex, presubiculum, and parasubiculum to the medial thalamus in macaque monkeys: identifying different pathways using disconnection techniques. Exp. Brain Res. 167 (1), 1–16.

Schiff, N.D., 2008. Central thalamic contributions to arousal regulation and neurological disorders of consciousness. Ann. N. Y. Acad. Sci. 1129, 105–118.

Schiff, N.D., 2010. Recovery of consciousness after brain injury: a mesocircuit hypothesis. Trends Neurosci. 33 (1), 1–9.

Schiff, N.D., Giacino, J.T., Kalmar, K., Victor, J.D., Baker, K., Gerber, M., Fritz, B., Eisenberg, B., Biondi, T., O'Connor, J., Kobylarz, E.J., Farris, S., Machado, A., McCagg, C., Plum, F., Fins, J.J., Rezai, A.R., 2007. Behavioural improvements with thalamic stimulation after severe traumatic brain injury. Nature 448 (7153), 600–603.

Sherman, S.M., Guillery, R.W., 2001. Exploring the Thalamus. Academic Press.

Shmueli, G., Patel, N., Bruce, P., 2010. Data mining for business intelligence: concepts, techniques, and applications in Microsoft Office Excel with XLMiner, 2nd ed. Wiley, Hoboken, NJ.

Smith, S.M., 2002. Fast robust automated brain extraction. Hum. Brain Mapp. 17, 143–155.

Smith, S., De Stefano, N., Jenkinson, M., Matthews, P., 2001. Normalized accurate measurement of longitudinal brain change. J. Comput. Assist. Tomogr. 25, 466–475.

Smith, S.M., Zhang, Y., Jenkinson, M., Chen, J., Matthews, P.M., Federico, A., De Stefano, N., 2002. Accurate, robust and automated longitudinal and cross-sectional brain change analysis. Neuroimage 17, 479–489.

Smith, S.M., Jenkinson, M., Woolrich, M.W., Beckmann, C.F., Behrens, T.E., Johansen-Berg, H., Bannister, P.R., De Luca, M., Drobnjak, I., Flitney, D.E., Niazy, R.K., Saunders, J., Vickers, J., Zhang, Y., De Stefano, N., Brady, J.M., Matthews, P.M., 2004. Advances in functional and structural MR image analysis and implementation as FSL. Neuroimage 23, S208–S219.

Street, J.O., Carroll, R.J., Ruppert, D., 1988. A note on computing robust regression estimates via iteratively reweighted least squares. Am. Stat. 42 (2), 152–154.

Studholme, C., Cardenas, V., Schuff, N., Rosen, H., Miller, B., Weiner, M., 2001. Detecting spatially consistent structural differences in Alzheimer's and fronto temporal dementia using deformation morphometry. Medical Image Computing and Computer-Assisted Intervention–MICCAI 2001. Springer, pp. 41–48.

Teasdale, G., Jennett, B., 1974. Assessment of coma and impaired consciousness: a practical scale. Lancet 304 (7872), 81–84.

Thompson, P.M., Giedd, J.N., Woods, R.P., MacDonald, D., Evans, A.C., Toga, A.W., 2000. Growth patterns in the developing brain detected by using continuum mechanical tensor maps. Nature 404 (6774), 190–193.

Van der Werf, Y.D., Jolles, J., Witter, M.P., Uylings, H.B.M., 2003. Contributions of thalamic nuclei to declarative memory functioning. Cortex 39 (4–5), 1047–1062.
van Groen, T., Kadish, I., Wyss, J.M., 2002. The role of the laterodorsal nucleus of the thalamus in spatial learning and memory in the rat. Behav. Brain Res. 136 (2), 329–337.
Wang, L., Swank, J.S., Glick, I.E., Gado, M.H., Miller, M.I., Morris, J.C., Csernansky, J.G., 2003. Changes in hippocampal volume and shape across time distinguish dementia of the Alzheimer type from healthy aging. Neuroimage 20 (2), 667–682.
Watanabe, Y., Funahashi, S., 2004. Neuronal activity throughout the primate mediodorsal nucleus of the thalamus during oculomotor delayed-responses. I. Cue-, delay-, and response-period activity. J. Neurophysiol. 92 (3), 1738–1755.
Watanabe, Y., Funahashi, S., 2012. Thalamic mediodorsal nucleus and working memory. Neurosci. Biobehav. Rev. 36 (1), 134–142.
Werner, C., Engelhard, K., 2007. Pathophysiology of traumatic brain injury. Br. J. Anaesth. 99 (1), 4–9.
Wilson, S.L., 1998. Magnetic-resonance imaging and prediction of recovery from post-traumatic vegetative state. Lancet 352 (9126), 485.
Woods, R.P., 2003. Characterizing volume and surface deformations in an atlas framework: theory, applications, and implementation. Neuroimage 18 (3), 769–788.
Yamamoto, T., Katayama, Y., Obuchi, T., Kobayashi, K., Oshima, H., Fukaya, C., 2013. Deep brain stimulation and spinal cord stimulation for vegetative state and minimally conscious state. World Neurosurg. 80 (3–4), S30.e1–S30.e9.
Yanovsky, I., Thompson, P.M., Osher, S., Leow, A.D., 2008. Asymmetric and symmetric unbiased image registration: statistical assessment of performance. IEEE Computer Society Conference on. IEEE, pp. 1–8.
Yanovsky, I., Leow, A.D., Lee, S., Osher, S.J., Thompson, P.M., 2009. Comparing registration methods for mapping brain change using tensor-based morphometry. Med. Image Anal. 13 (5), 679–700.
Zhang, Y., Brady, M., Smith, S.M., 2001. Segmentation of brain MR images through a hidden Markov random field model and the expectation maximization algorithm. IEEE Trans. Med. Imaging 20, 45–57.